Appl. Phys. B 67, 357–361 (1998)

Applied Physics B
Lasers
and Optics

Mid-infrared spectroscopic detection of trace gases using guided-wave difference-frequency generation

K.P. Petrov, A.T. Ryan, T.L. Patterson, L. Huang, S.J. Field, D.J. Bamford

Gemfire Corporation, 2471 East Bayshore Road, Suite 600, Palo Alto, CA 94303, USA
(Fax: +1-650/849-6900, E-mail: djbamford@aol.com)

Received: 1 April 1998/Revised version: 29 April 1998

Abstract. We report spectroscopic detection of methane and water vapor using mid-infrared difference-frequency generation of diode lasers in channel waveguides at room temperature. Waveguides with two different designs were fabricated using annealed proton exchange in periodically poled lithium niobate. One waveguide produced tunable radiation between 3.33 μm and 3.73 μm and the other produced tunable radiation between 2.65 μm and 2.90 μm. High-resolution spectra of methane (at 6.7 kPa) and water vapor (in ambient air) were obtained using electronically controlled frequency scans of up to 65 GHz. The use of diode lasers and highly efficient waveguide frequency converters in conjunction with fiber coupling will permit construction of compact, solid-state, room-temperature, mid-infrared sources for use in trace-gas detection.

PACS: 42.65.Wi; 07.07.Df; 42.72.Ai

Mid-infrared laser absorption spectroscopy is a promising technique for environmental trace-gas detection because many important air contaminants have strong absorption bands in that spectral region. This promise has not been fully realized because of practical drawbacks of the available laser sources including large size, high cost, limited tuning range, and the need for cryogenic cooling. Recent developments in semiconductor lasers, nonlinear optical materials, and integrated optics are making possible a new type of mid-infrared laser source that suffers from none of these difficulties.

Semiconductor lasers, operating at wavelengths between 0.6 μm and 2.0 μm, produce tunable narrowband radiation with output powers of 5–500 mW at room temperature. Environmentally important trace gases, however, generally do not have strong absorption lines in this wavelength region. Nonlinear optical techniques such as difference-frequency generation (DFG) and optical parametric oscillation (OPO) can be used to produce tunable radiation at longer wavelengths from these lasers. In recent years quasi-phase-matching (QPM) has been shown to allow much more efficient nonlinear frequency conversion than the more traditional technique, birefringent phase matching. The highest conversion efficiencies have been obtained using periodically poled lithium niobate (PPLN) as the nonlinear material [1, 2]. The creation of waveguides on the surface of the nonlinear optical material, using fabrication techniques borrowed from integrated optics [3, 4], leads to further enhancement of the conversion efficiency. Tight containment of light in a waveguide eliminates the trade-off between spot size and interaction length, in contrast to beams focused into bulk crystals. The combination of QPM and integrated optics allows efficient frequency conversion of cw lasers in the 100-mW class [1, 5], thus making it possible to build a compact, solid-state, room-temperature, mid-infrared source for use in trace-gas detection.

The remainder of this paper is organized as follows. In Sect. 1 the design of a tabletop mid-infrared spectrometer is given. The fabrication process for the most important component of the spectrometer, the PPLN waveguide, is described in Sect. 2. The usefulness of the system for spectroscopic gas detection is presented in Sect. 3. The prospects for a portable gas sensor based on quasi-phase-matched waveguide DFG are discussed in Sect. 4. Section 5 summarizes and concludes the paper.

1 Guided-wave DFG spectrometer

Figure 1 shows a schematic diagram of a difference-frequency spectrometer using a PPLN waveguide pumped by two tunable diode lasers. The pump laser was a tapered semiconductor amplifier seeded by an optically isolated external-cavity diode laser, with a single-frequency tuning range of 775 to 795 nm and 500 mW output power (SDL Inc., Model TC40). The signal laser was an external-grating-stabilized tapered semiconductor oscillator (SDL Inc., Model 8630) at 1010 nm with 250 mW of output power in single-frequency operation. This combination of pump and signal wavelengths was used to obtain a difference-frequency (idler) output in the 3.33–3.73 μm range for detection of methane. Later in the experiment, the signal laser was replaced by a similar unit with 500 mW of output power at 1096 nm to generate idler wavelengths of 2.65–2.90 μm suitable for detection of water vapor. Pump and signal beams were coupled into separate single-mode fibers. After polarization control, they were launched into one fiber using a fused coupler. With both

wavelengths available at the output of one connectorized fiber ("Y" in Fig. 1), it was possible to switch quickly between two different arrangements for coupling light into a PPLN waveguide. Initially we used a fiber-to-free-space collimating lens assembly followed by a microscope objective. By using a set of interchangeable, parfocal microscope objectives, we were able to obtain the desired spot size at the waveguide input without any changes in alignment. Later in the experiment, we butt-coupled light from a connectorized fiber by mounting the connector ferrule on a high-fidelity translation stage and bringing it close to the waveguide. Initial laser power was limited to 200 mW at each wavelength in order to prevent damage to the fiber-optic delivery system, rated at 400 mW.

The waveguide was operated at room temperature, without active temperature control. Powers of 50 mW at the pump wavelength and 100 mW at the signal wavelength were delivered to the waveguide input. A maximum waveguide throughput of 36% at 780 nm and 28% at 1096 nm were measured after adjustment of beam delivery optics to separately optimize the launched power at each wavelength. These throughputs are given without correction for Fresnel losses. We were unable to quantify the contributions of mode mismatch and optical absorption/scattering losses to these measured throughputs.

Idler radiation emerging at the output of the waveguide was collimated by a calcium fluoride lens with a focal length of 5 mm. The idler beam was then separated from the pump and signal beams by a germanium filter. An uncoated zinc selenide (ZnSe) wedge directed a portion of the idler beam onto an indium antimonide (InSb) reference detector. The remainder of the idler beam passed through a 30-cm-long stainless steel cell containing 1 to 20 kPa of methane at room temperature. The windows of the cell were crossed 3° wedges of calcium fluoride. The transmitted idler beam was then focused onto an InSb signal detector by an off-axis parabolic mirror. Both detectors were operated in a photovoltaic mode and cooled with liquid nitrogen.

The chopped signal from each infrared detector was measured by a separate lock-in amplifier. Quadrature outputs of the lock-in amplifiers were recorded by a digital oscilloscope that divided the signal voltage by the reference voltage. The ratio was displayed as a function of time, synchronized with the frequency scan of the pump laser. Residual radiation at the pump and signal wavelengths, available at the secondary output of the fused coupler ("X" in Fig. 1), was measured by a wavemeter with 1.5 GHz resolution (Burleigh Inc., Model WA-20).

2 Waveguide fabrication and performance

The centerpiece of the spectrometer in Fig. 1 is the PPLN waveguide. Two sets of 2-cm-long channel waveguides were fabricated in *z*-cut lithium niobate using annealed proton exchange [3, 4]. First, two commercial wafers of lithium niobate (75 mm in diameter, 0.5 mm thick) were patterned with a variety of QPM periods between 17.4 μm and 20.1 μm using electric field poling [6]. The QPM period mask was fabricated using a commercial pattern generator with 0.05-μm accuracy. Second, a chrome mask pattern was applied to the wafers to produce 6-μm- and 9-μm-wide channel openings, after which the wafers were diced. The wafer chips were proton-exchanged in pure benzoic acid and annealed in air. Table 1 presents a summary of exchange and anneal conditions for the two waveguide types.

A quasi-phase-matching curve of an annealed 6-μm waveguide, acquired by tuning of the pump laser from 775 to 795 nm, is shown in Fig. 2. Although a single grating period of 18.6 μm is used, the phase-matching curve contains multiple peaks because of the multiple waveguide spatial modes at the pump and signal wavelengths. For a given set of interaction wavelengths $\lambda_{p,s,i}$ that satisfy the energy conservation relation,

$$1/\lambda_p - 1/\lambda_s - 1/\lambda_i = 0, \tag{1}$$

the poling period Λ required for quasi-phase-matching of the TM_{00} waveguide modes is shorter than it would be for an interaction in bulk crystal because of the increased dispersion in the waveguide structure. A smaller shift occurs for interaction between higher order modes at the pump and signal wavelengths which have mode index values $N_{p,s,i}$ closer to that of the substrate.

$$N_p/\lambda_p - N_s/\lambda_s - N_i/\lambda_i - 1/\Lambda = 0 \quad . \tag{2}$$

For example, the difference-frequency mixing of 786 nm and 1010 nm (idler wavelength of 3.54 μm) in bulk lithium nio-

Table 1. Exchange and anneal conditions for two waveguide types

Design wavelength	PPLN period	Channel width	Exchange condition	Annealing condition
3.5 μm	18.6 μm	6 μm	170 °C, 24 h	340 °C, 34 h
2.7 μm	18.6 μm	9 μm	160 °C, 24 h	340 °C, 24 h

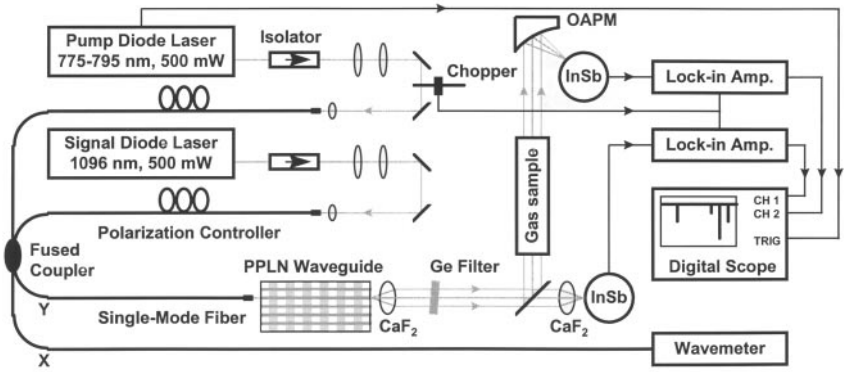

Fig. 1. Schematic diagram of a diode-pumped difference-frequency spectrometer using a PPLN waveguide. Two different ways of coupling laser light into a waveguide were used. Shown is the setup in which light was butt-coupled from a single-mode fiber

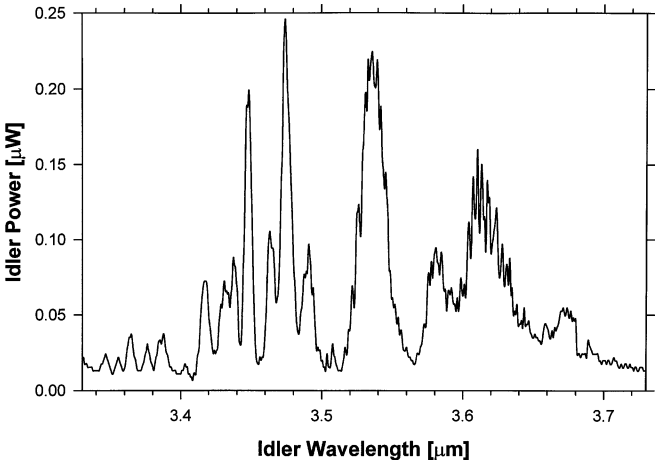

Fig. 2. DFG output power versus wavelength for a 6-μm channel waveguide in 18.6-μm periodically poled lithium niobate. The pump laser was tuned from 780 to 795 nm, while the signal laser was fixed at 1010 nm. Interaction of multiple spatial modes in the waveguide is evident from the multiple peaks in the phase-matching curve

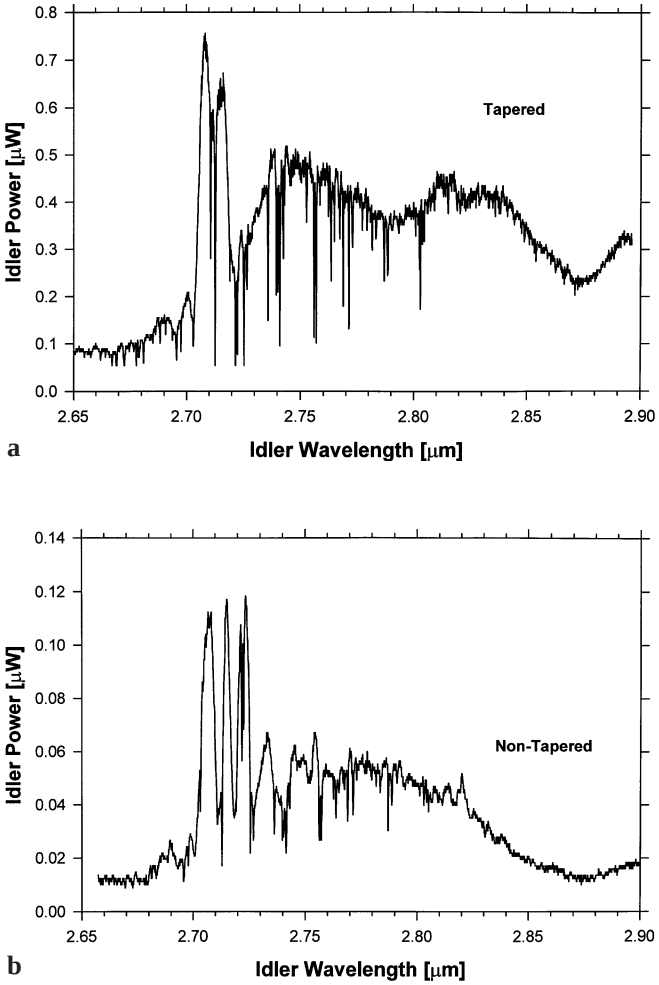

Fig. 3a,b. DFG output power versus wavelength for a 9-μm channel waveguide **a** with and **b** without an input taper. The pump laser was tuned from 775 to 795 nm, while the signal laser was fixed at 1096 nm. Both waveguides carry a PPLN grating period of 18.6 μm. Higher coupling efficiency and preferred excitation of the fundamental TM_{00} mode is evident for the tapered waveguide. Absorption by ambient water vapor can be seen in each trace

bate at room temperature would require a poling period of 21.3 μm [7]. In contrast, quasi-phase-matching of the same wavelengths in the waveguide is observed with a poling period of 18.6 μm. Our model calculations indicate that the waveguide supports 22 spatial modes at 780 nm and 10 spatial modes at 1010 nm. Due to the limited accuracy of the model, we were unable to identify the spatial modes that interacted to produce the multiple peaks in Fig. 2. The observed typical wavelength spacing of 0.01–0.03 μm between the peaks is, however, consistent with the model.

A method introduced by Chou et al. [8] was used to achieve efficient excitation of the fundamental waveguide mode at the pump and signal wavelengths. One half of all the 9-μm-wide waveguides were preceded by a 3-mm-long, 5-μm-wide input channel, and a 2-mm-long $5 \rightarrow 9$-μm linear width taper, both segmented with a period of 20 μm. The segment duty cycle increased parabolically from 20% at the input of the tapered section to 100% (non-segmented) at the output. Mid-infrared phase-matching curves of a tapered waveguide and a similar non-tapered waveguide, acquired by coarse tuning of the pump laser from 775 to 795 nm, are shown in Fig. 3. The two waveguides were examined under the same light-coupling condition: the laser light was focused from free space by a $6.3\times$ microscope objective. Higher input coupling efficiency was achieved with a tapered waveguide because of better mode-size matching between the focused beam and the periodically segmented input section. Significant output is observed primarily at two closely spaced idler wavelengths (Fig. 3a), because the waveguide input section supports two spatial modes at 780 nm. In contrast, the non-tapered waveguide (Fig. 3b) allows excitation of multiple modes at both pump and signal wavelengths, leading to a decrease in peak idler power.

The maximum idler power measured at the output of the tapered waveguide in Fig. 3a was 0.77 μW at 2.7 μm, with 11 mW launched pump power and 16 mW launched signal power. The overall device length was 25 mm, of which 20 mm was the length of the mixing section. Based on these data, the normalized DFG conversion efficiency of $\eta = 0.11\%\mathrm{W}^{-1}\mathrm{cm}^{-2}$ is calculated. Given the approximate $\eta \propto \lambda_i^{-4}$ scaling law, this result compares well with $\eta = 0.31\%\mathrm{W}^{-1}\mathrm{cm}^{-2}$ at 2.08 μm reported earlier by Arbore et al. [1]. Both these numbers are, however, significantly lower than $\eta = 6\%\mathrm{W}^{-1}\mathrm{cm}^{-2}$ which we estimate from an overlap integral [9] of TM_{00} modes at the pump and signal wavelengths. This estimate uses spatial mode profiles calculated from measured refractive index profiles of planar waveguides prepared using the same recipe. The estimate was calculated in the absence of linear absorption losses and imperfections in the waveguide structure and the PPLN grating.

The normalized conversion efficiency at 3.5 μm observed for the non-tapered 6-μm solid channel waveguide (see Fig. 2) was much lower, $0.01\%\mathrm{W}^{-1}\mathrm{cm}^{-2}$, primarily because of the distribution of pump and signal power among multiple spatial modes of the waveguide.

3 Spectroscopic measurements

To prove the usefulness of diode-pumped, guided-wave DFG for quantitative gas detection, the source described above was used to obtain high-resolution spectra of water vapor in

ambient air and of methane at low pressure. Fine-frequency scans of the pump laser system were performed by rotation of a diffraction feedback grating in its master oscillator, driven by a piezoelectric actuator. The rate of this electromechanical tuning could be varied between 0.2 and 20 sweeps per second, with peak-to-peak frequency excursion of up to 65 GHz. Since absolute accuracy of the measurement of pump and signal wavelengths was 3 GHz, the frequency axis in each absorption spectrum was calibrated by matching peak positions to their frequency assignments in the HITRAN database [10]. In addition to axis calibration, this procedure allowed us to investigate the linearity of frequency excursion versus control voltage applied to the piezoelectric actuator. The transfer function was linear to within 600 MHz except at the points where the direction of sweep was reversed. Figure 4 shows a portion of the water vapor spectrum near 3650 cm^{-1}, measured over a 27-cm open path in air. The solid trace was calculated for the water vapor partial pressure of 8.6×10^{-3} atm, equivalent to 31% relative humidity at 23 °C. The root-mean-squared magnitude of high frequency noise in the measured spectrum is 0.004, equivalent to a water vapor column density of 3 ppm m. The full-scale signal-to-noise ratio of 250 is limited by the presence of interference fringes in the signal and reference beam paths after the beamsplitter. Unlike power fluctuations and fringes introduced before the beamsplitter, these cannot be eliminated by the simple power ratio technique used in our experiment.

The fine-tuning range of 65 GHz, available in our instrument and typical of grating-tuned external-cavity diode lasers, is sufficient for monitoring a single pressure-broadened absorption line of water vapor. It is also sufficient for the purpose of high-resolution molecular spectroscopy [11]. Figure 5 shows a spectrum of methane at a pressure of 6.7 kPa (50 Torr) in a 30-cm absorption cell. From the observed magnitude and width of absorption peaks, we concluded that the idler linewidth exceeded the Doppler-broadened linewidth of methane at 3.5 μm. The solid trace shown in Fig. 5 is a convolution of a 500-MHz full width at half maximum Lorentzian profile with a methane absorption spectrum computed using

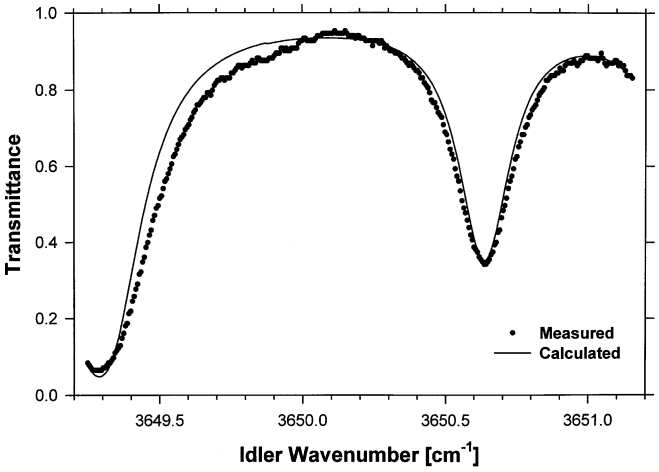

Fig. 4. Absorption spectrum of water vapor measured over 27-cm path in air. The circles plot a ratio of the signal and reference voltages, both recorded during a 2.5-s single sweep with a lock-in amplifier time constant of 30 ms. The solid trace was calculated for 31% relative humidity at 23 °C using the HITRAN database

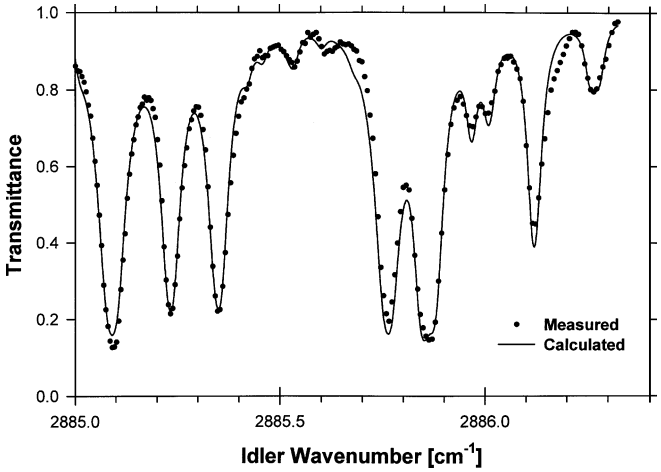

Fig. 5. Absorption spectrum of methane at 6.67 kPa (50 Torr) in a 30-cm-long cell. The circles plot a ratio of the signal and reference traces, both recorded as a 16-sweep average. Each sweep, performed at a 0.5-Hz rate, was detected by a lock-in amplifier with 10-ms time constant. The solid trace is a spectrum calculated using the HITRAN database and convoluted with a Lorentzian profile with a full width at half maximum of 500 MHz

the HITRAN database [10]. The convolution accounts well for the observed broadening of absorption lines and, more importantly, for the fact that the observed transmission is always well above zero. This computation was unnecessary in the analysis of pressure-broadened lines of water vapor in Fig. 4. The amount of methane used here, however, should cause the transmission near 2885.8 cm^{-1} to drop below the detectable level if probed with a sufficiently narrow linewidth source. The source linewidth of 500 MHz, inferred from the methane spectroscopy, is attributed to acoustic noise in the grating-stabilized cavity of the signal laser at 1010 nm and may be verified with a sufficiently high-finesse scanning Fabry–Perot interferometer. In our experiment this noise was registered over the time scale of 10 ms, and was found to depend on the current setting of the signal laser. For example, the linewidth of 500 MHz estimated from the data in Fig. 5 is different from 240 MHz observed earlier in a similar measurement [11]. Although this linewidth may be considered insufficient for Doppler-limited spectroscopy, it is adequate for trace-gas detection in ambient air where pressure-broadened linewidths are typically several GHz. Earlier work in high-resolution DFG spectroscopy [12] shows that linewidths below 50 MHz can be obtained with proper selection of pump and signal sources.

4 Discussion

The previous section described the capabilities of a table-top guided-wave DFG spectrometer. Presently there is much room for improvement in design and performance of the instrument. Optimized design of the mixing channel and the input taper [1], combined with improved fabrication techniques [3], should permit the development of DFG waveguide devices with efficiencies approaching 25%W^{-1}. Such devices will permit generation of 25 μW mid-infrared output power with only 10 mW launched pump and signal power. Instrument packaging for wavelength-specific applications will allow improved coupling between the lasers and the wave-

guide and will raise the output power to the 250-μW level. At this level of output power, diode-pumped DFG sources may substitute lead-salt diode lasers in their usual spectroscopic applications. In this experiment, both detectors were cooled with liquid nitrogen. Portable instruments demanding more robust detectors could employ HgCdTe photoconductive cells that deliver comparable wavelength response, detectivity, and speed in a thermoelectrically cooled package [13, 14].

One of the key features of a PPLN DFG waveguide demonstrated in this work is its versatility. Figure 3a shows how close the waveguide is to idler cutoff, with the appearance of a broad DFG peak beginning at 2.7 μm. Based on the earlier investigation of parametric fluorescence in PPLN waveguides by Baldi et al. [9], this broad peak is attributed to phase-matched generation of an unguided idler wave, the Cerenkov-idler configuration. In the present work, and in a previous experiment in our laboratory [11], the unguided idler radiation was observed directly, in contrast to the earlier observation of the spectrally inverted signal wave in parametric fluorescence. Although a detailed image of the idler beam would present a more conclusive proof of observation of Cerenkov interaction, we were unable to perform it because of limited availability of equipment.

A wide range of Cerenkov-idler wavelengths at which appreciable DFG output power could be obtained in a single waveguide constitutes a potential benefit to spectroscopic applications. For example, the 2.65- to 2.90-μm wavelength region shown in Fig. 3 covers the entire P branch of the fundamental stretch-vibration band of water vapor, an important greenhouse gas. Absorption by water vapor in the beam path to the signal detector can be seen in both traces in Fig. 3. Thus a single waveguide design can be used with many pairs of pump and signal lasers to probe molecular absorption in a wide range of wavelengths. For example, detection of sulfur dioxide (SO_2) at 4.0 μm would become possible with the use of a 980-nm signal laser. Likewise, the mixing of an 810-nm pump laser and a 980-nm signal laser would produce the 4.7-μm light necessary for detection of carbon monoxide (CO). Regardless of waveguide design, its use in spectroscopy will require the aid of power stabilization [12] or the use of a reference arm in order to cancel out the variations in idler power as a function of wavelength.

Although the generation of an unguided idler is less efficient than truly guided wave DFG, it is more efficient than bulk DFG. For example, the observed peak unguided idler output of 0.55 μW in Fig. 3a corresponds to a normalized conversion efficiency of $0.15\%\mathrm{W}^{-1}\mathrm{cm}^{-1}$, which is higher than the $0.05\%\mathrm{W}^{-1}\mathrm{cm}^{-1}$ reported for 3-μm difference-frequency mixing in bulk PPLN by Goldberg et al. [15].

In addition to being more efficient than bulk DFG, Cerenkov DFG offers a unique feature. Namely, the wide tuning bandwith of a Cerenkov waveguide (see Fig. 3a) is instantaneous in that it is accessible by tuning the pump laser wavelength only. This is an important advantage over bulk DFG, where similar bandwidths are achieved by wavelength tuning in conjunction with either crystal rotation, crystal temperature tuning, or the use of multiple QPM gratings which require crystal translation – processes that are inherently slow.

5 Summary and conclusions

Tunable mid-infrared radiation was produced in the wavelength region of 2.65–2.90 μm and 3.33–3.73 μm by mixing a tunable diode laser near 780 nm with fixed-wavelength diode lasers at 1096 nm and 1010 nm in PPLN waveguides. Two sets of 2-cm-long waveguides, with channel widths of 6 μm and 9 μm, were manufactured using annealed proton exchange. The 9-μm waveguides were used in conjunction with a periodically segmented $5 \rightarrow 9$-μm linear width taper with a segment duty cycle variation from 20% to 100%. A single poling period of 18.6 μm was used for quasi-phase-matching in all waveguides. The maximum idler power generated at 2.7 μm was 0.77 μW, with 11 mW pump power and 16 mW signal power launched into a tapered waveguide, equivalent to the normalized conversion efficiency of $0.11\%\mathrm{W}^{-1}\mathrm{cm}^{-2}$. High-resolution spectroscopy of pure methane at 6.7 kPa and detection of water vapor in ambient air were performed in 2.5 s, showing good quantitative agreement between measured and calculated spectra. The results demonstrate the versatility and simplicity of a novel integrated-optic gas sensor based on quasi-phase-matched guided-wave difference frequency mixing of diode lasers at room temperature.

Acknowledgements. The authors would like to thank Kris Wolfe, Rosemary Lucero, Eric Darko, and Linda Whittelsey for their assistance in preparing the PPLN waveguide samples. This work was supported by the National Aeronautics and Space Administration, the Department of Energy, and the U.S. Air Force.

References

1. M.A. Arbore, M.-H. Chou, M.M. Fejer: CLEO'96 Technical Digest **10**, 120 (1996)
2. W.R. Bosenberg, A. Drobshoff, J.I. Alexander, L.E. Myers, R.L. Byer: Opt. Lett. **21**, 1336 (1996)
3. P.G. Suchoski, T.K. Findakly, F.J. Leonberger: Opt. Lett. **13**, 1050 (1988)
4. M.L. Bortz, M.M. Fejer: Opt. Lett. **16**, 1844 (1991)
5. E.J. Lim, H.M. Hertz, M.L. Bortz, M.M. Fejer: Appl. Phys. Lett. **59**, 2207 (1991)
6. S.J. Field, L. Huang, K. Wolfe, D.J. Bamford, D.A.G. Deacon: Paper TuT3 presented at the OSA Annual Meeting, October 1997. To be published in "Laser Applications and Issues", OSA Trends in Optics and Photonics, 1998
7. D.H. Jundt: Opt. Lett. **22**, 1553 (1997)
8. M.-H. Chou, M.A. Arbore, M.M. Fejer: Opt. Lett. **21**, 794 (1996)
9. P. Baldi, P. Aschieri, M. De Micheli, D.B. Ostrowsky, D. Delacourt, M. Papuchon: IEEE J. Quantum Electron. **31**, 997 (1995)
10. L.S. Rothman, R.R. Gamache, A. Goldman, L.R. Brown, R.A. Toth, H.M. Pickett, R.L. Poynter, J.-M. Flaud, C. Camy-Peyret, A. Barbe, N. Husson, C.P. Rinsland, M.A.H. Smith: Appl. Opt. **26**, 4058 (1987)
11. K.P. Petrov, A.T. Ryan, T.L. Patterson, L. Huang, S.J. Field, D.J. Bamford: Opt. Lett. **23**, 1052 (1998)
12. K.P. Petrov, S. Waltman, E.J. Dlugokencky, M.A. Arbore, M.M. Fejer, F.K. Tittel, L.W. Hollberg: Appl. Phys. B **64**, 567 (1997)
13. T. Topfer, K.P. Petrov, Y. Mine, D.H. Jundt, R.F. Curl, F.K. Tittel: Appl. Opt. **36**, 8042 (1997)
14. K.P. Petrov, R.F. Curl, F.K. Tittel: Appl. Phys. B **66**, 531 (1998)
15. L. Goldberg, W.K. Burns, R.W. McElhanon: Opt. Lett. **20**, 1280 (1995)